Aalto University

OPEN ACCESS

This is an electronic reprint of the original article.
This reprint may differ from the original in pagination and typographic detail.

Mahmoud, Karar; Lehtonen, Matti

Three-level control strategy for minimizing voltage deviation and flicker in PV-rich distribution systems

Published in:
International Journal of Electrical Power and Energy Systems

DOI:
10.1016/j.ijepes.2020.105997

Published: 01/09/2020

Document Version
Peer-reviewed accepted author manuscript, also known as Final accepted manuscript or Post-print

Published under the following license:
CC BY-NC-ND

Please cite the original version:
Mahmoud, K., & Lehtonen, M. (2020). Three-level control strategy for minimizing voltage deviation and flicker in PV-rich distribution systems. *International Journal of Electrical Power and Energy Systems*, *120*, Article 105997. https://doi.org/10.1016/j.ijepes.2020.105997

This material is protected by copyright and other intellectual property rights, and duplication or sale of all or part of any of the repository collections is not permitted, except that material may be duplicated by you for your research use or educational purposes in electronic or print form. You must obtain permission for any other use. Electronic or print copies may not be offered, whether for sale or otherwise to anyone who is not an authorised user.

Three-level control strategy for minimizing voltage deviation and flicker in PV-rich distribution systems

Karar Mahmoud*, Matti Lehtonen

Department of Electrical Engineering and Automation, Aalto University, FI-00076 Espoo, Finland

Abstract

Voltage deviation (VD) and voltage flicker (VF) are considered common operational problems associated with high photovoltaic (PV) penetrated distribution systems. In this paper, an optimal control strategy is proposed for minimizing VD and VF in PV-rich distribution systems. The control strategy is based on proposed analytical expressions that minimize both voltage problems by optimizing the smart functions of the PV inverters and control devices simultaneously. The proposed analytical expressions are formulated based on voltage sensitivities with respect to the active and reactive power injections of PV. Specifically, a three-level control strategy with different time resolutions is proposed to significantly alleviate voltage deviation/flicker while minimizing PV active power curtailments and tap movements for transformers. These control levels are 1) local control (LC), 2) area control (AC), and 3) coordinated control (CC). LC provides rapid local control actions to minimize VD and VF, AC minimizes VD within the corresponding area individually, and CC plays a vital role to coordinate between the various control units. The proposed control strategy is assessed using high PV penetration with realistic high-resolution very-variable solar radiation datasets (10 milliseconds). To demonstrate the accuracy and

*Corresponding author at: Department of Electrical Engineering and Automation, Aalto University, FI-00076 Espoo, Finland

Email address: karar.mostafa@aalto.fi, matti.lehtonen@aalto.fi (Karar Mahmoud, Matti Lehtonen)

efficiency of the proposed analytical expressions, the calculated results have been compared with existing methods. Results demonstrate that the proposed control strategy effectively coordinates between the various voltage control units while minimizing VD and VF.

Keywords: Distribution systems; photovoltaic; voltage deviation; voltage flicker; control strategy; analytical expressions.

1. Introduction

Integrating various renewable energy sources as distributed energy resources (DER) in LV/MV distribution systems is an effective worldwide strategy for decreasing greenhouse gas emissions. Renewable DERs have significantly uncompetitive features compared with traditional energy sources, e.g., lower costs, better supply reliability, lower losses, and enhanced power quality [1–3]. Driven by these benefits, the use of renewable DERs has been globally expanded in recent years. One of the fastest-growing DERs is photovoltaic (PV) generation systems where their contribution is expected to reach 11% of global electricity generation by 2050 [4], [5]. Nevertheless, high penetration of such renewable DERs can degrade the performance and efficiency of distribution systems due to their highly fluctuating generation [6–8].

One of the most serious operational problems with high PV penetration is voltage deviations (VD). Voltage flicker (VF) also represents another operational problem caused by the abrupt change of the PV generation during transient clouds. To quantify VF with PV, various IEEE and IEC standards have been developed [9], [10]. These two associated phenomena with PV can greatly degrade the performance of distribution systems and harm interconnected instruments [11–14]. In addition, the lifetime of traditional voltage control devices, such as on-load tap changer transformer (OLTC), step voltage regulator (SVR), and capacitor bank (CB), could be reduced due to the infrequent operation of their tap mechanism

[15–19]. To solve these issues locally, several developments have been accomplished in advanced voltage control architectures that employ the smart functionalities of the PV inverter [20–23]. These functionalities include reactive power control and active power curtailment. Driven by these benefits, the recent revised IEEE 1547 Standard and grid codes of many countries require the utilization of such smart functionalities of PV inverters for voltage support [24,25]. Besides, oversizing the interface inverters of PV units is a possible way to release their spare capacity for wider local control options [26,27].

Various methods have been presented in the literature for solving the voltage violation and flicker problems with high PV penetration. In [28], the ramp-rate from PV has been recommended to be within 10% of the nominal rate per minute to reduce the impacts of voltage flickers. The authors of [29] have proposed a piecewise linear function based on historical information for computing the local optimal reactive power of PV inverters to keep the voltage within permissible limits. A combined central and local control scheme of active and reactive power of PV inverters while respecting system limitations has been presented in [30]. Based on the reactive power capability and real power curtailment of PV inverters, a comprehensive optimal control strategy of PV has been introduced in [31] to improve the performance of distribution networks including voltage profiles with high PV penetrations. In [32], besides the total active curtailed PV power curtailment, the charging power of electric vehicles has been incorporated in the voltage control optimization model. Droop-based algorithms for controlling the PV active power curtailment have been utilized in [33] to avoiding voltage rise in distribution systems. The authors of [34] have developed a voltage control strategy while minimizing curtailed PV power. In [35], the severe effects of various parameters of clouds on voltage flicker have been quantified and investigated. The options to curtail PV power and control the PV inverter reactive power, respectively, have been utilized in [36] and [37] to reduce voltage flickers. Energy storage devices have been employed in

[38] to manage the PV inverter ramp-rate within a preset level. Other special components have been utilized in other studies, e.g. supercapacitors [39], DERs [40], electrical vehicles [41] and [42], multi agent system [43], and damp loads [44]. Most of the existing control methods treat VD or VF individually while a unified treatment for these two correlated problems is essential. Farther, reactive power support of PV inverter (complying with the IEEE 1547 Standard), transformer taps, curtailed power, and various constraints are needed to be incorporated in the control scheme.

As stated above, several operation problems are associated with PV-rich distribution systems, including VD, VF, high tap movement, and high active power curtailment of PV. To solve these issues, an optimal control strategy for PV-rich distribution systems is proposed in this work. Unlike the existing methods, the proposed strategy optimizes both VD and VF while minimizing the active power curtailment of PVs and the number of tap movements for transformers in a simultaneous manner. To do so, the proposed control strategy involves three control levels with different time resolutions: local control (LC), area control (AC), and coordinated control (CC). New analytical expressions with a high accuracy rate and light computational burden are formulated to be employed in LC and AC. As a result, LC and AC could rapidly minimize VD and VF via optimizing active/reactive PV generation. Regarding CC, an optimal power flow (OPF) formulation is developed and used in this unit to coordinate between various controllers according to voltage levels and active PV power curtailments. Based on such a cooperative control scheme, the proposed strategy is capable of performing proper control actions for OLTC, SVRs, and inverters of PVs along the grid and so completely solve the operational problems with high PV penetrations. In addition, the proposed strategy is a flexible tool to make a trade-off between various benefits, i.e., VD minimization, VF minimization, reducing tap movements, and decreasing PV active power curtailment. The efficiency of the proposed strategy is demonstrated on a 119-bus distribution system interconnected to high PV penetration with realistic high-resolution very-variable solar radiation datasets.

2. Proposed formulation

Here, new analytical expressions are proposed for minimizing VD and VF problems in distribution systems by optimizing the smart functions of the PV inverters and various control devices. The proposed analytical expressions are based on voltage sensitivities with respect to the active and reactive power injections of PV.

2.1. Formulae for local VF Minimization

Here, analytical expressions are introduced to directly calculate the optimal local reactive power injections for mitigating local VF (LVF). Such flickers are caused by irradiance transients and load variations. The proposed analytical expressions are based on voltage sensitivities with respect to the power injections. Fig. 1 describes a general distribution line model in which a PV unit and a certain load are connected to its receiving node. At time instant t_m, the voltage magnitude at the receiving node (V_r) is expressed as a function of the line impedance (Z_{sr}=R_{sr} + jX_{sr}), the voltage at the sending bus (V_s), and active/reactive power flows through the distribution line as follows:

$$V_r(t_m) = V_s(t_m) - VD_{sr}(t_m) \tag{1}$$

in which

$$VD_{sr}(t_m) = \left(R_{sr} + j\,X_{sr}\right)\left(\frac{P_r^{In}(t_m) + j\,Q_r^{In}(t_m)}{V_r(t_m)}\right)^{*} \tag{2}$$

$$\begin{cases} P_r^{In}(t_m) = \underbrace{P_r^{LD}(t_m) - P_r^{PV}(t_m)}_{P_r^{Inj}(t_m)} + P_r^{Out}(t_m) \\ Q_r^{In}(t_m) = \underbrace{Q_r^{LD}(t_m) - Q_r^{PV}(t_m)}_{Q_r^{Inj}(t_m)} + Q_r^{Out}(t_m) \end{cases} \tag{3}$$

where VD_{sr} represents the voltage drop between s and r buses. $\left(P_r^{In}, Q_r^{In}\right)$ and $\left(P_r^{Out}, Q_r^{Out}\right)$ denote incoming active and reactive powers to bus r and the sum of transmitted active and reactive powers from bus r to the downstream lines, respectively. $\left(P_r^{PV}, Q_r^{PV}\right)$ and $\left(P_r^{LD}, Q_r^{LD}\right)$ denote active and reactive powers of PV and the load at bus r, respectively. By decomposing the real and imaginary parts of (2), the real and imaginary parts of the voltage at the receiving node can be expressed as follows:

$$\begin{bmatrix} V_r^{\mathrm{Re}}(t_m) \\ V_r^{\mathrm{Im}}(t_m) \end{bmatrix} = \begin{bmatrix} \alpha_{sr}(t_m) & \beta_{sr}(t_m) \\ -\beta_{sr}(t_m) & \alpha_{sr}(t_m) \end{bmatrix} \begin{bmatrix} V_s^{\mathrm{Re}}(t_m) \\ V_s^{\mathrm{Im}}(t_m) \end{bmatrix} \tag{4}$$

where

$$\begin{cases} \alpha_{sr}(t_m) = 0.5 + \sqrt{0.25 - \dfrac{P_r(t_m)R_{sr} + Q_r(t_m)X_{sr}}{\left(V_s^{Abs}(t_m)\right)^2} - \beta^2(t_m)} \\ \beta_{sr}(t_m) = \left(P_r(t_m)X_{sr} - Q_r(t_m)R_{sr}\right) \Big/ \left(V_s^{Abs}(t_m)\right)^2 \end{cases} \tag{5}$$

Since the LVF is represented by the voltage magnitude, the line model can be expressed as follows:

$$V_r^{Abs}(t_m) = \chi_{sr}(t_m) V_s^{Abs}(t_m) \tag{6}$$

where $V_s^{Abs}(t_m)$ and $V_r^{Abs}(t_m)$ represent the voltage magnitude at the sending and receiving bus, where $\chi_{sr}(t_m) = \sqrt{\alpha_{sr}^2(t_m) + \beta_{sr}^2(t_m)}$.

Then, a formula is introduced to calculate the required injected/consumed reactive power of the local PV inverter to compensate LVF. This formula is based on the sensitivity of the reactive power with respect to the active power of the PV unit. The initial value of the PV reactive power ($Q_r^{PV,Int}$) can be formulated as follows:

$$Q_r^{PV,Int}(t_{m+1}) = Q_r^{PV}(t_m) + \frac{\partial Q_r^{PV}(t_m)}{\partial P_r^{PV}(t_m)} \left(P_r^{PV}(t_{m+1}) - P_r^{PV}(t_m)\right) \tag{7}$$

where

$$\frac{\partial Q_r^{PV}(t_m)}{\partial P_r^{PV}(t_m)} = \frac{\partial V_r^{Abs}(t_m)}{\partial P_r^{PV}(t_m)} \times \frac{\partial Q_r^{PV}(t_m)}{\partial V_r^{Abs}(t_m)}$$
$$= \frac{\alpha_{sr}(t_m)\frac{\partial \alpha_{sr}(t_m)}{\partial P_r^{PV}(t_m)} + \beta_{sr}(t_m)\frac{\partial \beta_{sr}(t_m)}{\partial P_r^{PV}(t_m)}}{\alpha_{sr}(t_m)\frac{\partial \alpha_{sr}(t_m)}{\partial Q_r^{PV}(t_m)} + \beta_{sr}(t_m)\frac{\partial \beta_{sr}(t_m)}{\partial Q_r^{PV}(t_m)}} \tag{8}$$
$$= \frac{\frac{\alpha_{sr}(t_m)\left(R_{sr} + 2X_{sr}\beta_{sr}(t_m)\right)}{\alpha_{sr}(t_m) - 0.5} - 2X_{sr}\beta_{sr}(t_m)}{\frac{\alpha_{sr}(t_m)\left(X_{sr} - 2R_{sr}\beta_{sr}(t_m)\right)}{\alpha_{sr}(t_m) - 0.5} + 2R_{sr}\beta_{sr}(t_m)}$$

Equation (8) can be employed for smoothing voltage fluctuations caused by the intermittent PV active power generation. The computational burden of this proposed formula is very light, and so it is applicable for real-time control. Note that if the computed reactive power is higher than the spare capacity of the inverter $\left(Q_r^{PV,Max}(t_m) = \sqrt{\left(S_r^{PV}(t_m)\right)^2 - \left(P_r^{PV}(t_m)\right)^2}\right)$, its value must be limited to this constraint. Then, the reactive power of PV is corrected using the following formula:

$$Q_r^{PV,Com}(t_{m+1}) = Q_r^{PV,Int}(t_{m+1}) + Q_r^{PV,Cor}(t_{m+1}) \tag{9}$$

where

$$Q_r^{PV,Cor}(t_{m+1}) = \frac{\partial Q_r^{PV}(t_m)}{\partial V_r^{Abs}(t_m)}\left(V_r^{Abs,Est}(t_{m+1}) - V_r^{Abs}(t_m)\right) \tag{10}$$

where $Q_r^{PV,Com}$ and $Q_r^{PV,Cor}$ represent the compensating reactive power of PV and the corrected PV reactive power. This correction which is computed by (10) aims to reduce the difference between the past voltage value and the estimated voltage value $V_r^{Abs,Est}$. Note that the estimated voltage is calculated by (6) for each PV bus considering the initial calculated PV reactive power ($Q_r^{PV,Int}$).

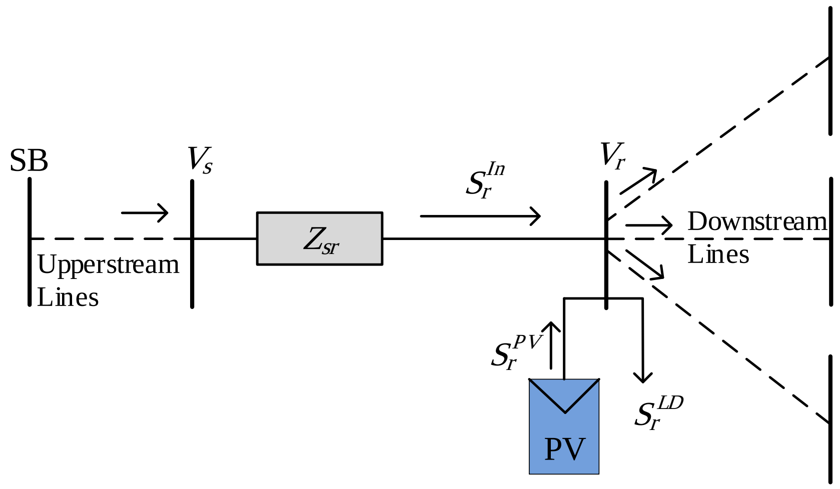

Fig. 1. Line model of distribution systems with PV.

2.2. Formulae for VD minimization

Here, we introduce analytical formulae to calculate the optimal PV generation so as to minimize the total voltage drop through the distribution lines, i.e. VD minimization. The control scheme of PV considers the smart functionalities of the interfaced inverter which comprises reactive power compensation and active power curtailment.

2.2.1. VD formula

The absolute of the voltage deviation for a distribution line at the base case (without considering PV) be approximated to:

$$VD_{sr0} \cong \alpha_r P_r^0 + \beta_r Q_r^0 \tag{11}$$

where

$$\begin{cases} \alpha_r = \dfrac{R_{sr}}{V_r^{Abs}} \\ \beta_r = \dfrac{X_{sr}}{V_r^{Abs}} \end{cases} \tag{12}$$

The total normalized voltage deviation through all distribution lines (TVD_0) can be expressed as follows:

$$TVD_0 = \sum_{r \in \Omega_B} \left(\alpha_r P_r^0 + \beta_r Q_r^0\right)^2 \tag{13}$$

where Ω_B includes a list of all system lines.

2.2.2. Total VD with PV

The formula of total VD (TVD) is reformulated here to be as a function of the active/reactive injected power of PV. Consider a 12-bus distribution system in which the load demand is fed by the main distribution substation represented as the slack bus (SB), as shown in Fig. 2(a). The TVD for this system can be calculated directly by (13). Nevertheless, the value of TVD will be significantly varied if PV is connected to the system. In such a situation, considering the superposition theorem, the active/reactive PV power generation will follow the direct path to the SB since the load demand is constant. For example, as illustrated in Fig. 2(b), the generated power of the two added PV units will flow the shown direct two paths to SB due to the radial structure of the system. In general, a formula to calculate TVD with a single PV unit at bus *i* can be expressed as follows:

$$TVD_{PV} = \sum_{r\in\Omega_{B1}} \left(\alpha_r P_r^0 + \beta_r Q_r^0\right)^2 + \sum_{r\in\Omega_{B2}} \left(\alpha_r P_r^D + \beta_r Q_r^D\right)^2 \tag{14}$$

in which

$$\begin{cases} P_r^D = P_r^0 - P_i^{PV} \\ Q_r^D = Q_r^0 - Q_i^{PV} \end{cases} \tag{15}$$

where Ω_{B1} includes a list of branches belonged to the direct path of the PV unit to the slack bus while the Ω_{B1} list includes the other branches, where $\Omega_{B1} \cup \Omega_{B1} = \Omega_B$. This formula helps to directly quantify the contribution of each individual PV unit in TVD minimization.

Consider that a number of PV units are connected to a list of buses $\left(\Omega_{PV}\right)$ a distribution system. To compute voltage deviation in this case, equation (15) is modified as follows:

$$\begin{cases} P_r^D = P_r^0 - \sum_{i\in\Omega_{PV}} C_{i,r} P_i^{PV} \\ Q_r^D = Q_r^0 - \sum_{i\in\Omega_{PV}} C_{i,r} Q_i^{PV} \end{cases} \tag{16}$$

where C_{ir} is equal to 1 if the branch r belongs to the upper-stream path of the PV unit at bus i; otherwise it equals 0. For example, the binary matrix **C** for the distribution system shown in Fig. 2 (b) can be written as follows:

$$\mathbf{C} = \begin{array}{c} \overbrace{\begin{array}{cccccccccccc} 1 & 2 & 3 & 4 & 5 & 6 & 7 & 8 & 9 & 10 & 11 & 12 \end{array}}^{System\ Buses} \\ \begin{bmatrix} 1 & 1 & 1 & 0 & 1 & 1 & 1 & 0 & 0 & 0 & 0 & 0 \\ 1 & 1 & 1 & 0 & 0 & 0 & 0 & 0 & 1 & 1 & 1 & 0 \end{bmatrix} \end{array} \left. \begin{array}{l} 7 \\ 11 \end{array} \right\} PV\ Buses$$

The incorporation of the powers of multiple PV units in the TVD formula enables to assess the voltage directly without iterative processes. This formula is utilized in each area controller for TVD evaluation considering the PV units in each corresponding area.

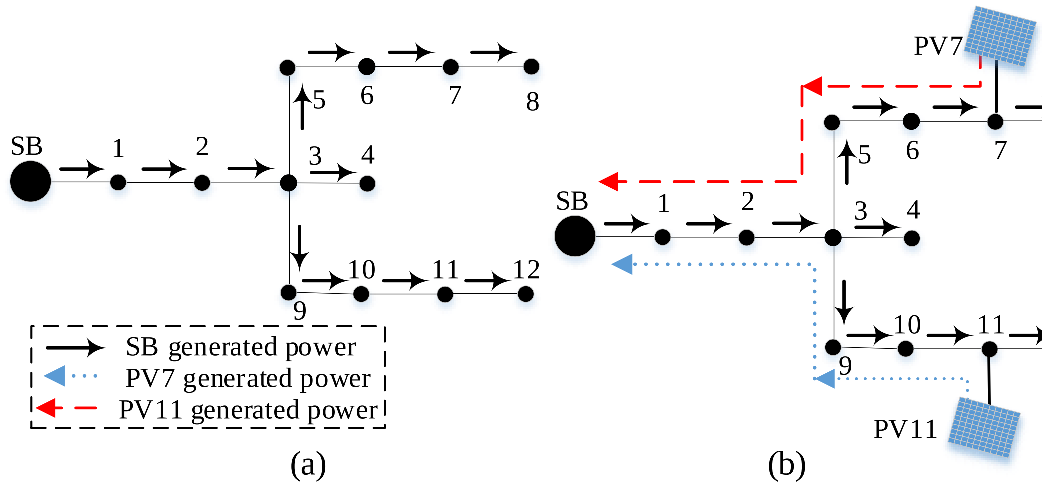

Fig. 2. Power flow variation with PV. (a) Power flows without PV, and (b) Power flows with two PV units.

2.2.3. Analytical expressions for reactive power control

Here, we propose analytical expressions to compute the reactive power of the various DERs including PV, dispatchable DER, and reactive power sources so as to minimize TVD. As the slope of the TVD function with respect to the reactive powers of DERs is zero at its optimal value, the following equation is satisfied for each DER at bus m:

$$\frac{\partial TVD_{DER}}{\partial Q_m^{DER}} = -2 \sum_{r \in \Omega_{B2}} C_{m,r} \beta_r \left(\alpha_r P_r^0 + \beta_r \left(Q_r^0 - \sum_{i \in \Omega_{DER}} C_{i,r} Q_i^{DER} \right) \right) = 0 \quad (17)$$

Rearranging (17) yields:

$$\sum_{r\in\Omega_{B2}} C_{m,r}\beta_r\beta_r\left(\sum_{i\in\Omega_{DER}} C_{i,r}P_i^{DER}\right)=\sum_{r\in\Omega_{B2}} C_{m,r}\beta_r\left(\alpha_r P_r^0+\beta_r Q_r^0\right) \tag{18}$$

The above equation can be written for each DER. These set of equations are set in matrix form as follows:

$$\begin{bmatrix} Q_1^{DER} \\ \vdots \\ Q_N^{DER} \end{bmatrix}=\begin{bmatrix} \phi_{1,1} & \cdots & \phi_{1,N} \\ \vdots & \ddots & \vdots \\ \phi_{N,1} & \cdots & \phi_{N,N} \end{bmatrix}^{-1}\begin{bmatrix} \varphi_1 \\ \vdots \\ \varphi_N \end{bmatrix} \tag{19}$$

where

$$\begin{cases} \phi_{n,m}=\sum_{r\in\Omega_{B2}} C_{n,r}\beta_r^2 C_{m,r} \\ \varphi_m=\sum_{r\in\Omega_{B2}} C_{m,r}\beta_r\left(\alpha_r P_r^0+\beta_r Q_r^0\right) \end{cases} \tag{20}$$

By using (19) and (20), direct optimal solutions for the reactive power of the various DER types are computed to minimize TVD. Note that the computed reactive power is constrained with the maximum limit of DERs while considering the practical operation zones for some DERs (i.e., switched capacitors).

2.2.4. Analytical expressions for active power control

Proposed analytical expressions are formulated for computing the optimal real power curtailment of PV and the optimal real power output of dispatchable DERs to minimize TVD. Similar to (17) and (18), the following two equations are satisfied at the optimal TVD with respect to the real power of DER at bus *m*:

$$\begin{aligned}\frac{\partial TVD_{DER}}{\partial P_m^{DER}}&=-2\sum_{r\in\Omega_{B2}} S_{m,r}\alpha_r\left(\alpha_r\left(P_r^0-\sum_{i\in\Omega_{DER}} S_{i,r}P_i^{DER}\right)+\beta_r Q_r^0\right)\\&=0\end{aligned} \tag{21}$$

$$\sum_{r\in\Omega_{B2}} S_{m,r}\alpha_r\alpha_r\left(\sum_{i\in\Omega_{DER}} S_{i,r}P_i^{DER}\right)=\sum_{r\in\Omega_{B2}} S_{m,r}\alpha_r\left(\alpha_r P_r^0+\beta_r Q_r^0\right) \tag{22}$$

Rearranging these set of equations are set in matrix form:

$$\begin{bmatrix} P_1^{DER} \\ \vdots \\ P_N^{DER} \end{bmatrix} = \begin{bmatrix} \phi_{1,1} & \cdots & \phi_{1,N} \\ \vdots & \ddots & \vdots \\ \phi_{N,1} & \cdots & \phi_{N,N} \end{bmatrix}^{-1} \begin{bmatrix} \varphi_1 \\ \vdots \\ \varphi_N \end{bmatrix} \tag{23}$$

in which

$$\begin{cases} \phi_{n,m} = \sum\limits_{r\in\Omega_{B2}} S_{n,r}\alpha_r^2 S_{m,r} \\ \varphi_m = \sum\limits_{r\in\Omega_{B2}} S_{m,r}\alpha_r\left(\alpha_r P_r^0 + \beta_r Q_r^0\right) \end{cases} \tag{24}$$

These analytical expressions calculate the optimal active power of multiple DER units. For a dispatchable DER, the computed active power using (23) has optimal value to maximize TVD while it is constrained by the generation capability. However, for a PV unit, after computing its optimized generated active power using (23), the active power curtailment $\left(P_i^{PVC}\right)$ can be computed by:

$$P_i^{PVC} = \begin{cases} P_i^{PVA} - P_i^{PV} & P_i^{PV} < P_i^{PVA} \,\&\, P_i^{PVA} - P_i^{PV} \le P_i^{PVC,Max} \\ 0 & P_i^{PV} > P_i^{PVA} \\ P_i^{PVC,Max} & P_i^{PV} < P_i^{PVA} \,\&\, P_i^{PVA} - P_i^{PV} \ge P_i^{PVC,Max} \end{cases} \tag{25}$$

where P_i^{PVA} and $P_i^{PVA,Max}$ stands for the available active power of PV with respect to the environmental condition and the maximum allowed PV power to be curtailed, respectively.

3. Formulation of the coordinated control

Here, the optimization model of the CC unit is described. Specifically, it comprises three sub-objective functions that quantify voltage violation (VV), tap movement rate (TMR) of transformers, and the total active curtailed power (ACP) of PVs. The objective function is formulated at time instant t_s as follows:

$$F(t_s) = \left(VV(t_s),\ TMR(t_s),\ ACP(t_s)\right) \tag{26}$$

in which the sub-objectives are described below.

$$VV(t_s) = \sum_{i\in\Omega_{VV}} \left(W_{VV,i}(t_s) \times \left(V_i^L(t_s) - V_i(t_s) \right)^2 \right) \tag{27}$$

$$TMR(t_s) = \sum_{p=1}^{N} \sum_{k\in\gamma} \left(W_{TMR,k}(t_s) \times \left(\frac{T_k(t_s) - T_k(t_{s-p})}{T_{k,step}} \right)^2 \right) \tag{28}$$

$$ACP(t_s) = \sum_{m\in\eta} F_{APC,m}(t_s) \times \left(P_i^{PVA} - P_i^{PV} \right)^2 \tag{29}$$

where $VV(t_s)$ represents voltage violation at time t_s, Ω_{VV} includes a list of nodes at which the voltage exceeds the upper/lower limits $\left(V_i^L(t_s)\right)$, and $W_{VV,i}$ represents a weight factor of node i, where $\sum_{i\in\Omega_{VV}} W_{VV,i} = 1$. Equation (28) models TMR of transformers, where $T_k(t_s)$ and $T_k(t_{s-p})$ represent the tap position of transformer k at time t_s and that of the previous time t_{s-p}, respectively; γ stands for the list of transformers in the distribution system; $T_{k,step}$ is the step value of the tap mechanism for transformer k; N is the number of past time instants considered in the present time instant t_s. $W_{TMR,k}$ represents a weight factor of transformer k, where $\sum_{k\in\gamma} W_{TMR,k}(t_s) = 1$.

Indeed, the decision to curtail the active power of PV can prevent voltage rise. The total ACP in a power distribution system is formulated by (29). η is PV buses. W_{APC} stands for the weight factor of the active power curtailment of each PV unit. The utilization of the three sets of weight factors in the three sub-objectives gives more flexibility to system operators for comprehensive control actions.

For this optimization model, the next constraints are considered:

$$P_m^{PVC}(t_s) \le CPR_{\max,m} \times P_m^{PV,\max}(t_s), \qquad \forall m \in \eta \tag{30}$$

$$\begin{aligned} &-\sqrt{\left(\left(O_m^{PV} S_m^{PVR}\right)^2 - \left(P_m^{PVA}(t_s) - P_m^{PVC}(t_s)\right)^2 \right)} \le Q_m^{PV}(t_s) \\ &\le \sqrt{\left(\left(O_m^{PV} S_m^{PVR}\right)^2 - \left(P_m^{PVA}(t_s) - P_m^{PVC}(t_s)\right)^2 \right)}, \qquad \forall m \in \eta \end{aligned} \tag{31}$$

$$Tap_k^{min} \le Tap_k(t_s) \le Tap_k^{max}, \quad \forall k \in \gamma \tag{32}$$

$$\left(Tap_k(t_{s-1}) - Tap_k(t_s)\right) / Tap_{k,step} \le TapR_k, \quad \forall k \in \gamma \tag{33}$$

The constraint (30) represents the upper boundary $\left(CPR_{max}\right)$ of the normalized active power curtailment of each PV unit. The constraint (31) denotes the rise of the spare capacity of the interfaced inverter, whose rated capacity is S^{PVR}, considering the curtailed power. As a result, further reactive power compensation can be injected/absorbed to be employed by the controllers for voltage deviation/flicker mitigation. The unique feature of the reactive power control is that it can rapidly respond to fast undesirable voltage variations due to cloud transient. Consequently, the PV inverter is assumed here to have the capability for providing reactive power supply within the spare inverter capacity. An important planning factor is considered in (31) that is the inverter oversized factor (O^{PV}) which provides wide active/reactive control options. The constraints (32) and (33) model the upper/lower limits of taps of transformers and maximum allowed tap movements ($TapR_k$) of each transformer, respectively.

Note that line parameters and power at system nodes are required to be known for applying the control strategy. For this purpose, the proposed control system is equipped with a data storage device, which is an essential component of the distribution management system (DMS), in which distribution system parameters are stored. Further, we considered that all nodes of the distribution system are equipped with smart meters, and so the power of the nodes can be monitored and shared with the control system. Note that this assumption is realistic, complying with the massive deployment of intelligent metering in the EU and worldwide [45].

4. Proposed Control Strategy

In this work, an efficient voltage control strategy is proposed to alleviate the voltage quality paradigm that comprises VD and VF while optimizing: 1) the stress on some voltage control devices (i.e., number of tap operations of transformers) and 2) active power curtailment of PV. At each control cycle, the state variables (i.e. voltage, power flows) are measured/estimated in the distribution system. For this purpose, we utilize the backward/forward sweep power flow method introduced in [46]. For each *Area x* in the distribution system, the following the voltage rise index (VRI), voltage drop index (VDI), and curtailed power index (CPI) are computed. VRI_x and VDI_x are equal to 1 if the voltage limits in *Area x* are violated; otherwise, no voltage violations exist. CPI_x is equal to 1 if the sum of active power curtailment of PVs in *Area x* exceeds the maximum preset limits by utilities; otherwise, it is zero. The control law of transformer *k* at *zone x* with for controlling voltage and regulating active PV power curtailment is formulated as follows:

$$Tap_{k,x}\left(t_s\right)=\begin{cases}Tap_{k,x}\left(t_{s-1}\right)+Tap_{k,Step} & VDI_x\left(t_s\right)=1\ \&\ Tap_x\left(t_{s-1}\right)<Tap_{k,x}^{\max}\\ Tap_{k,x}\left(t_{s-1}\right) & VDI_x\left(t_s\right)=0\ \&\ VRI_x\left(t_s\right)=0\\ Tap_{k,x}\left(t_{s-1}\right)-Tap_{k,Step} & VRI_x\left(t_s\right)=1\ \|\ CPI_x\left(t_s\right)=1\ \&\ Tap_x\left(t_{s-1}\right)>Tap_{k,x}^{\min}\end{cases} \tag{34}$$

The proposed strategy has three control levels with different time resolutions, as described below:

- ***Local control (10 milliseconds):*** It aims at providing rapid real-time local control actions to mitigate local voltage deviation and flicker at PV connection points considering smart functionalities of the interfaced inverter. Since this controller treats two conflicting sub-objectives (voltage deviations and flicker), the following control law is utilized based on the present voltage zone. At each time step, each individual control of a PV unit checks the current local voltage. If the voltage is within the normal voltage boundaries (i.e. *VRI* and *VDI* at PCCs are 0), the controller will mitigate LVF using (8)-(10). Otherwise, it minimizes the local voltage deviations using the mathematical formulation in Section 2.2, where the optimal active/reactive power of each PV is computed individually.

- ***Area control (*1 *sec):*** It provides optimal active and reactive power control of various DER types (PV, dispatchable DER, and reactive power sources) for each individual area in the distribution system to minimize the voltage deviation. To do so, this controller utilizes the proposed analytical expressions to compute the optimal contributions of all resources within the same area for minimizing VD in the case that VRI_x and VDI_x equal 1. As a result, the voltage level for each area is instantaneously enhanced by its cooperative DERs.
- ***Coordinated control (2 min):*** It performs a coordinated voltage control scheme whenever voltage violations and/or excessive active power curtailment of PV units are noticed, which are identified by VRI_x, VDI_x, and CPI_x. The proposed optimization model presented in Section 3 is employed in this control system. This control solves both of these issues while optimizing the number of tap operations of transformers in a simultaneous manner.

As illustrated above, the proposed control strategy contains various control stages at three different time resolutions which are repeated on each control cycle. **Algorithm 1** describes the proposed control strategy of distribution systems with PV.

Algorithm 1: Proposed control strategy
1: **Inputs**: Distribution system data, PV data, load demand, and the present tap status of transformers. 2: **Outputs**: Optimized control variables, including active power curtailment of PVs $\left(\mathrm{P}^{\mathrm{PVC}}=\left\{P_1^{PVC} \quad P_2^{PVC} \quad \ldots \quad P_n^{PVC}\right\}\right)$, reactive power of PVs $\left(Q^{\mathrm{PVC}}=\left\{Q_1^{PV} \quad Q_2^{PV} \quad \ldots \quad Q_n^{PV}\right\}\right)$ (**$\mathbf{Q}_{\mathbf{PV}}$**=$\{Q_{PV1}, Q_{PV2}, ..., Q_{PVn}\}$), and tap movements of transformers (Tap=$\{Tap_1, Tap_2, ..., Tap_n\}$), besides various state variables.

3: **Start Procedure:** Proposed Strategy
4: **For** each time step t_s **Do**
5: Mesure/compute current state variables, and calculate various indices
6: Activate the LC unit
7: **For** each *Area x*
8: **If** (VRI_x **OR** VDI_x**==** 1) **AND** the operation cycle of AC_x is attained **Then**
9: Activate the AC unit, apply control actions, and update the stored variables
10: **End If**
11: **End For**
12: **If** (*VRI* **OR** *VDI* **OR** *CPI* **==** 1) **AND** the CC operation cycle is attained **Then**
13: Activate the CC unit, apply control actions
14: **End if**
15: Save current state and control variables
16: **End For**
17: **End Procedure**

Note that we consider a real-time control scheme for the local control that reacts to the rapid change of the local active PV power generation due to cloud transients, in a time-scale of less than a second. This is applicable since the smart PV inverter dispatches quickly (cycle-to-cycle time scale) providing a local way for rapid voltage regulation without causing voltage instability problems [47]. The reason for selecting a time scale of 2 min for the OLTC is to ensure acceptable voltage profile and low active PV power curtailment during the day. Note that this narrow setting is important since it is the outer control level, but OLTC will not move unless voltage violations or higher PV curtailment (not often every 2 min), which cannot be solved by the first or the second control levels. Regarding the communication delay, it is normally very smaller than 1 sec. For example, machine-to-machine interaction in LTE network communication takes on average 20 ms [48,49]. Therefore, the communication delay will have small impacts on area control.

Here, exchange communication between the three-level control units is described. This issue is important for implementing the proposed control strategy in real distribution systems. For each area of the distribution system, the AC unit communicates with the LC units to exchange information about voltage conditions (identified by *VRI* and *VDI*), and active/reactive power of PVs. Note that there are no communication links among the AC units in the distribution system, like the LC units. However, the CC unit has communication links to all AC units for monitoring the voltage status and active PV power curtailment for each area of the distribution system and sending control commands. Based on the measurements and data which are synchronized using GPS, the proposed three-level control system determines proper control decisions and then communicates them to the various controllable devices.

5. Results and Discussions

5.1 Test system

A modified 119-node 11-kV test distribution system is utilized for validating the accuracy of the proposed analytical expressions and demonstrating the effectiveness of the proposed voltage control strategy. The line and load data of the original test system are given in [50]. As shown in Fig. 3, this studied distribution system involves three areas (1, 2 and 3), one OLTC unit, and three SVRs.

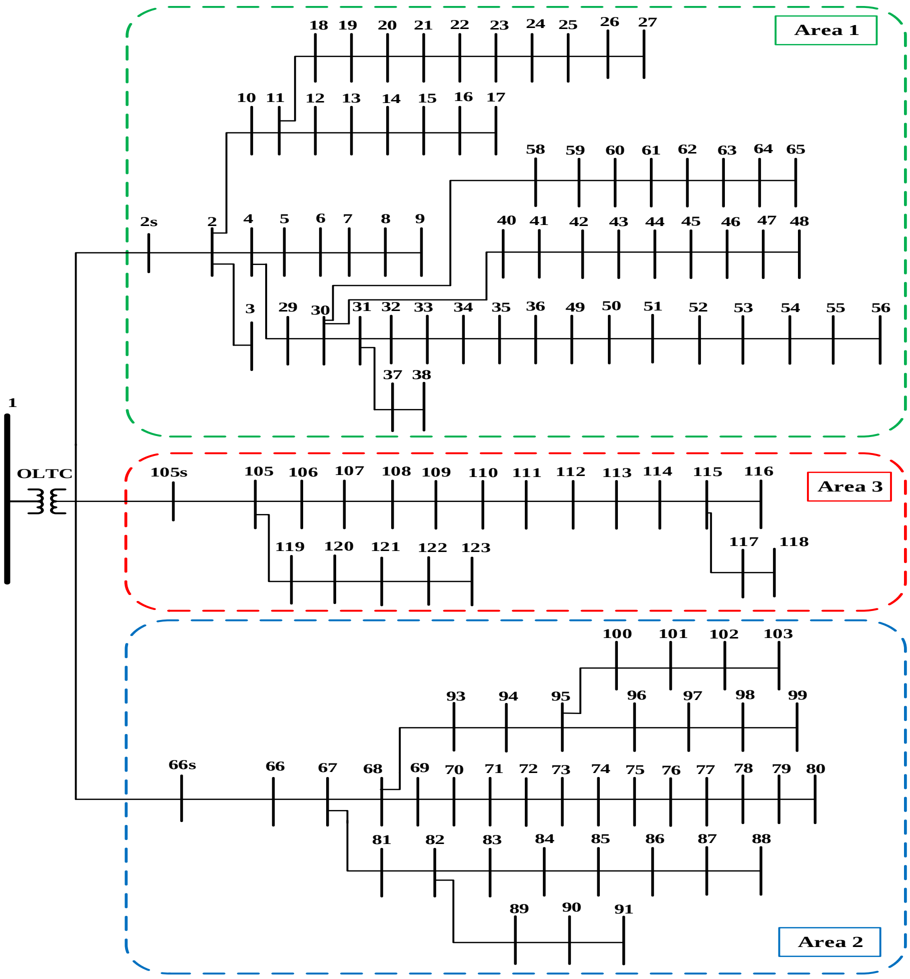

Fig. 3. The modified 119-bus distribution system.

5.2 Validation of the proposed formulae for TVD minimization

Here, we validate the accuracy of the proposed formulae for minimizing TVD by optimal DER active and reactive power control in the test system. Specifically, equations (19) and (23) are employed to compute the optimal reactive power and active power, respectively, to minimize TVD at the base loading condition. The calculated results by the proposed method are compared with exhaustive search solutions which represent a benchmark solution. Note that the topology, configuration, and loading conditions are kept the same as the base condition during this test.

Fig. 4 compares the computed optimal active and reactive DER power for TVD minimization and the corresponding TVD improvement (%) by proposed and exact methods.

Three DER scenarios are simulated: 1) one DER at bus 51, 2) two DERs at buses 51 and 80, and 3) three DERs at buses 51, 80 and 118. As shown, the calculated active and reactive power of DER for all scenarios are very close to those of the exact solutions. As a result, the value of TVD is minimized by the proposed formulae for the different DER scenarios, implying that the voltage profiles are optimally improved. It is also noted that a higher number of DERs leads to higher TVD improvement.

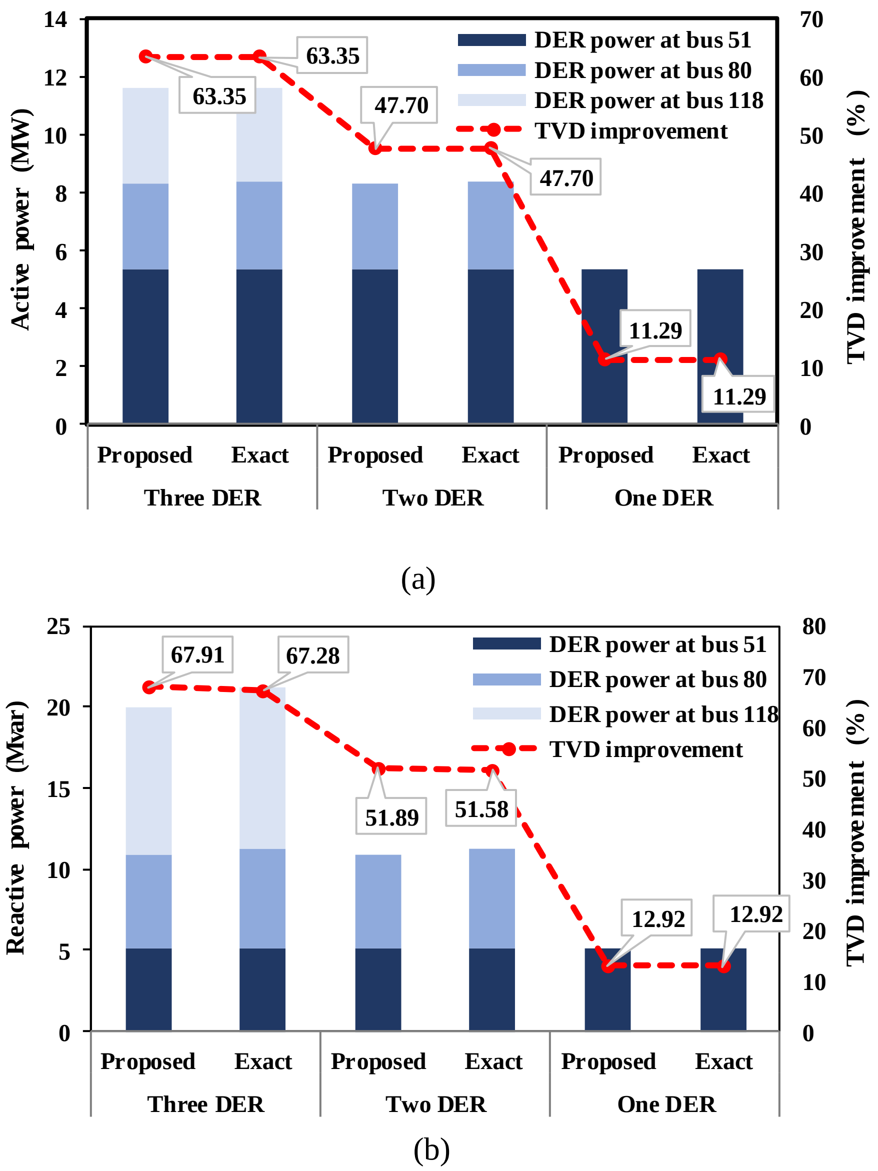

Fig. 4. Calculated optimal active and reactive DER power for TVD minimization at three DER cases, and the corresponding TVD by proposed and exact methods.

5.3 Validation of the proposed formulae for LVF minimization

To demonstrate the efficacy of the proposed formulae to minimize LVF, the DER reactive power is computed by (8)-(10) to compensate a specified variation in the active DER power. The DER active power is varied up to 2000 kW (with 500 kW step) for the three DER locations.

Fig. 5 shows the calculated reactive power at three locations with different DER active power variation for LVF minimization corresponding LVF values by the proposed method and the R/X method. As shown in Fig. 5 (a), the R/X method overestimates the DER reactive power for all locations, resulting in higher LVF values compared to the proposed method. This error in the R/X method increases by the amount of DER active power variation, as shown in Fig. 5 (b). Unlike the R/X method, the proposed method significantly minimizes LVFs, thanks to its comprehensive model.

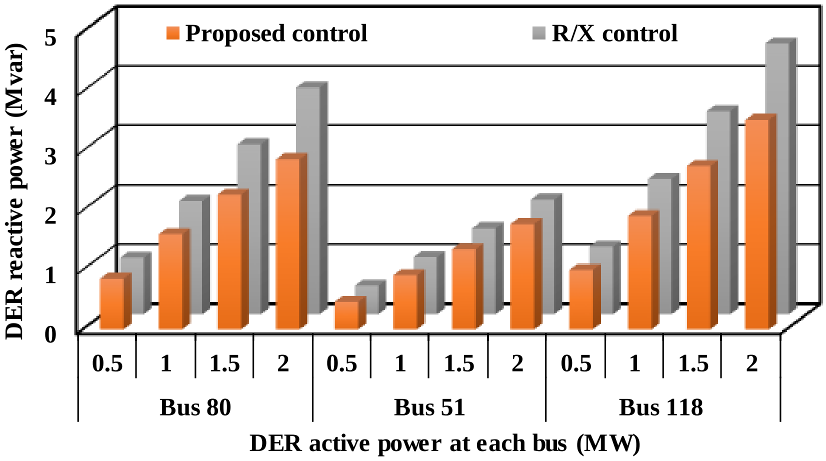

(a)

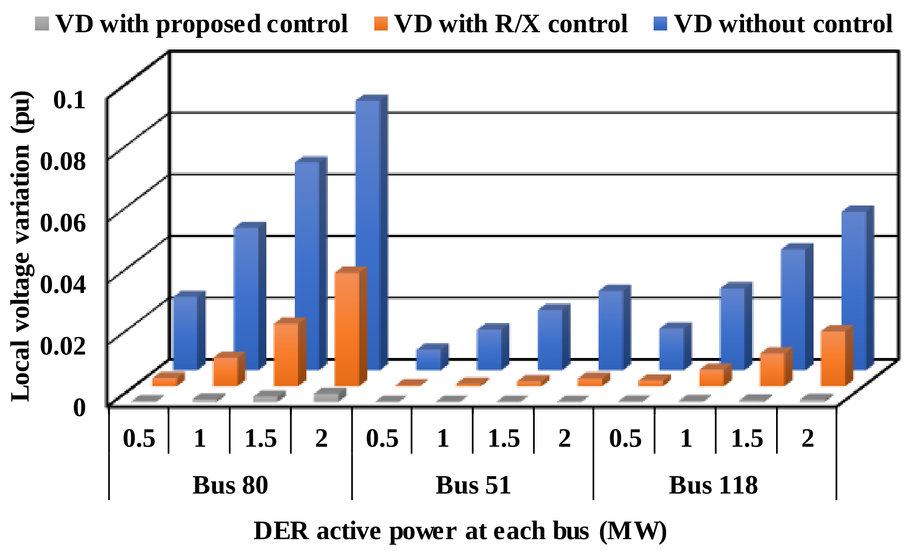

(b)

Fig. 5. Computed DER reactive power for LVF minimization with different DER active power at three locations and the corresponding LVFs by various methods.

5.4 Assessing the proposed voltage control strategy

In this assessment of the proposed strategy, intensive real-time simulation is performed on the 119-nodes test system with three PVs. The three PV units, i.e. PV1 at bus 51, PV2 at bus 80, and PV3 at bus 118, contain 300, 1200, 30000 modules (SHARP's NTR5E3E PV 175W), respectively. To simulate the highly intermittent nature of PV, a high-resolution solar radiation dataset is used [51]. Fig. 6 shows the profile of solar radiation where the resolution of the dataset is 10 milliseconds. Furthermore, various types of load demand are considered to be distributed in the 119-bus distribution system: domestic, industrial, lighting, and commercial profiles.

Fig. 7 shows the voltage profiles with a time resolution of 10 millisecond at points of common connection (PCCs) of the three PV units which are distributed among the three areas for the base case (i.e., without control). As noticed, the voltage in Area 3, in which PV3 is connected, exceeds the upper voltage boundary. On the contrary, voltage drop problems are noticed in Areas A and B where PV1 and PV2 are connected, respectively. During the midday, voltage rise and voltage drop problems have coexisted which require an efficient coordinated control scheme to be mitigated. Another issue to be noticed is the high rates of LVF, especially at the PCC of PV3.

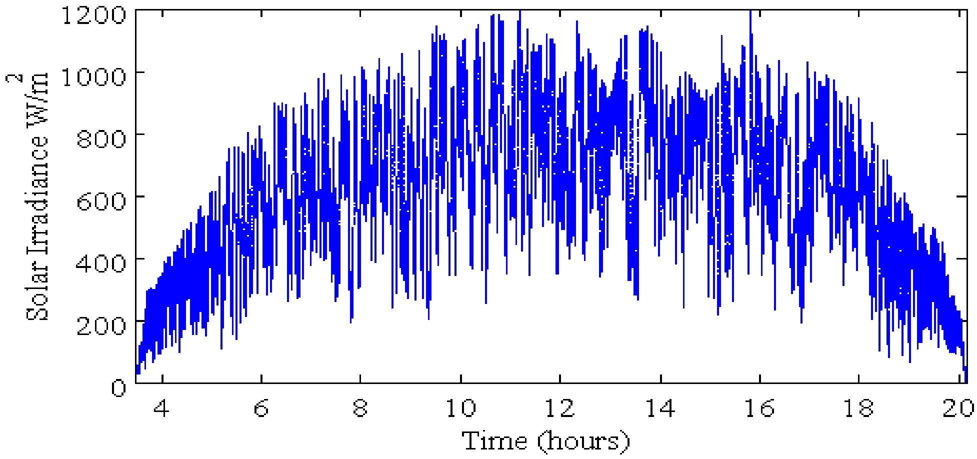

Fig. 6. Solar radiation profile (10 millisecond resolution).

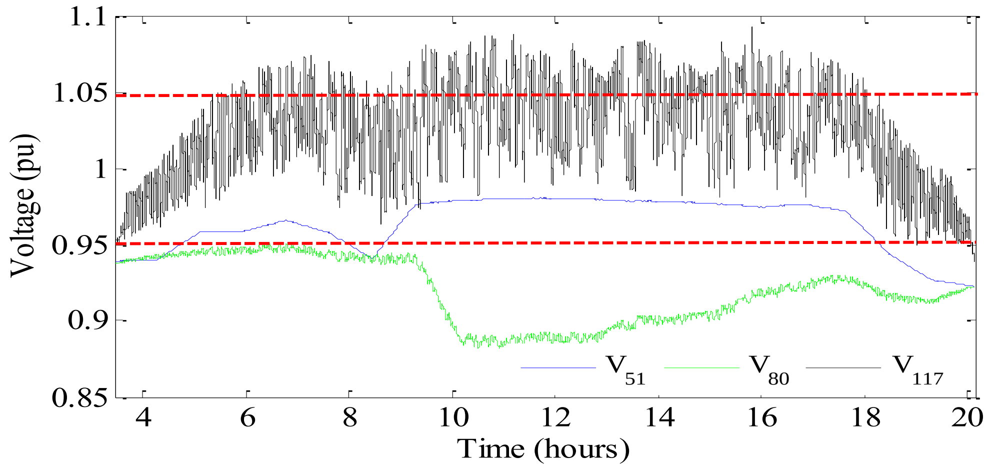

Fig. 7. Voltage profile at PCCs for the base case.

To show the effectiveness of the proposed control strategy, we compare the base PCC voltage profiles at the highest fluctuating and violating area (PCC of Area 3) with the R/X control and the proposed strategy. As shown in Fig. 8, the R/X control and the proposed control strategy reduce LVF and TVD with respect to the base case. However, the proposed strategy has much higher improvement rates in terms of minimizing LVF. This analysis reveals the superiority of the proposed formulation to minimize the LVF rate while regulating voltages.

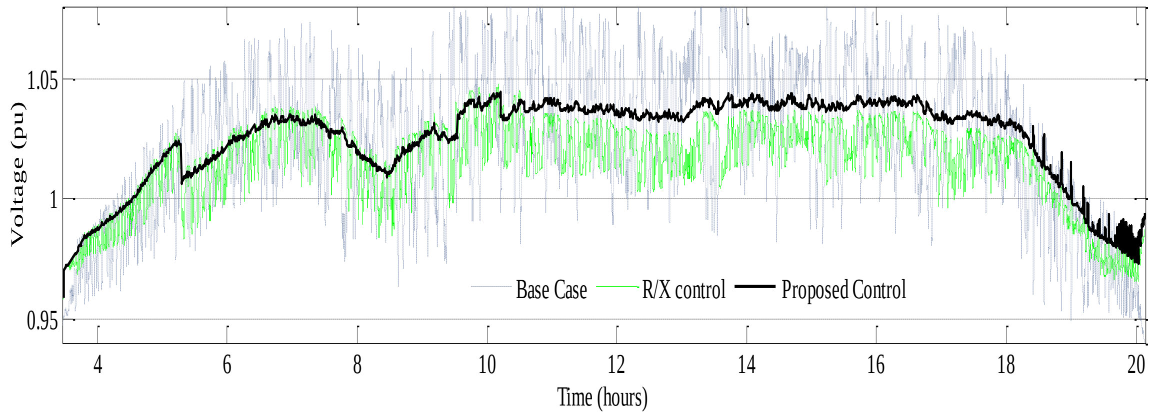

Fig. 8**.** Voltage profiles at bus 118 (PCC of area 3).

Fig. 9 shows the results of the proposed control strategy in terms of voltage profiles at PCCs, active PV power curtailment, reactive power of the PV inverters, and tap positions of transformers with a time resolution of 10 millisecond. It is obvious that the proposed strategy can solve both VD and VF problems for all buses at the three areas (see Figs. 9(a,b,c)) since the voltages are kept within the lower/upper limits, and the voltages are greatly smoothed. The calculated reactive power of the PV inverters shown in Fig. 9 (d) are highly fluctuating to solve VD and VF, but their values are within the spare capacity of the interfaced inverters. We can also notice that their values tend to be high during the midday in which the variation of active PV power is the highest. This is normal since the required reactive power to compensate VD and VF increases proportionally with respect to the active PV power variation. Regarding active PV power curtailments shown in Fig. 9(e), their values are kept small during the studied period by the CC unit. This unit monitors the voltage levels and active power curtailment, and when their values reached undesired range, it simultaneously adjusts the operating points of the various units via OPF. For instance, the CC unit moves the taps of transformers (Fig. 9(f)) around 10:00 to prevent high active power curtailment for voltage regulation. Another benefit of the proposed strategy is that the number of tap operations during the highly fluctuating PV profile is low, thanks to OPF which optimizes their operation number.

It is important to note that the proposed strategy is general and can adopt other grid codes of utilities. For example, the proposed strategy could be adjusted to prevent the active power curtailment, but this benefit will be on the expensive of higher operations of transformer taps. This voltage control strategy is also a helpful tool for distribution system operators and planners to investigate and test the potential operational problems with high PV penetration and explore comprehensive control-based solutions.

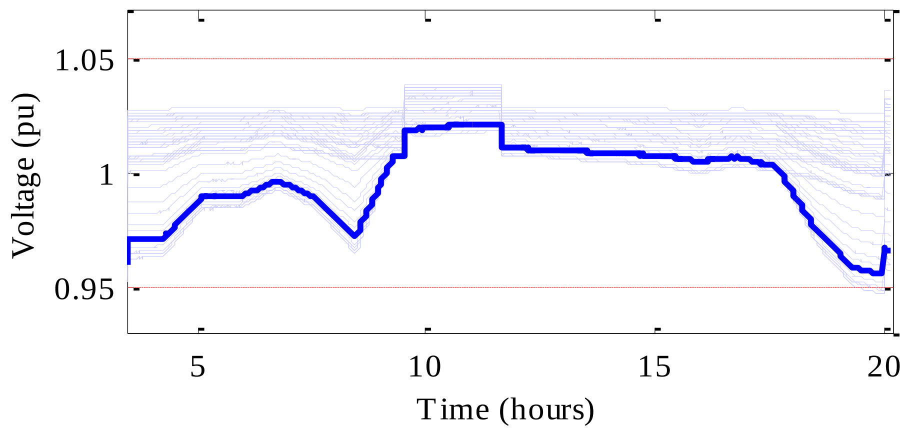

(a)

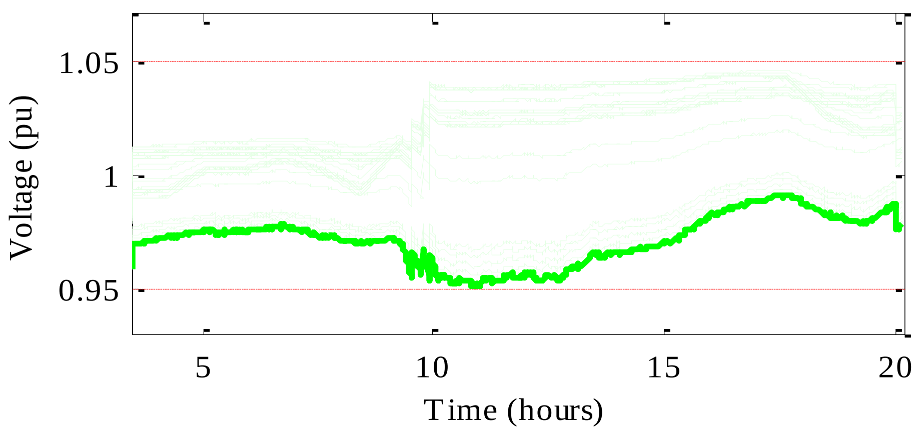

(b)

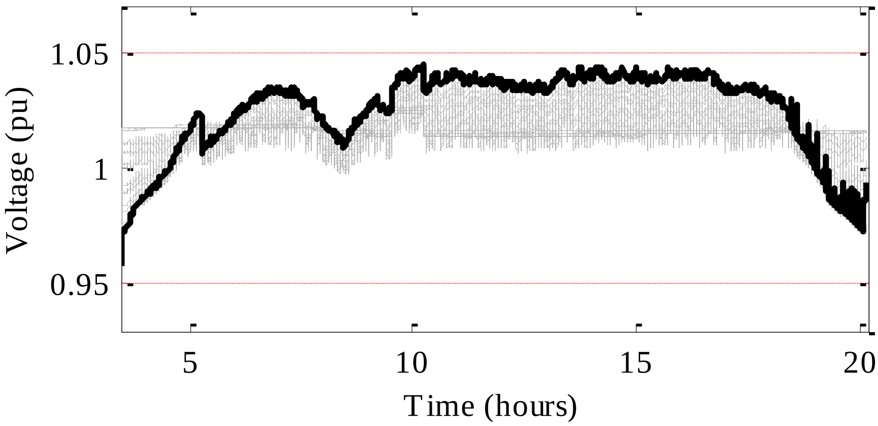
Voltage (pu)
1.05
1
0.95
5
10
15
20
Time (hours)

(c)

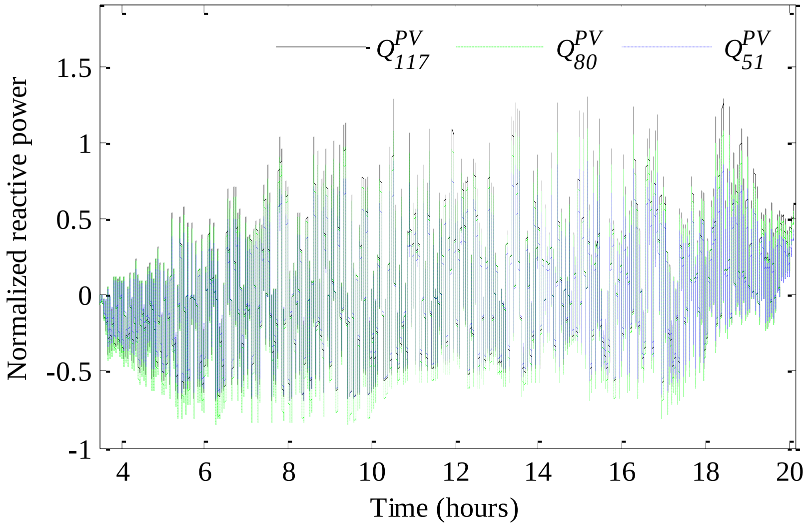
Q_{117}^{PV}
Q_{80}^{PV}
Q_{51}^{PV}
Normalized reactive power
1.5
1
0.5
0
-0.5
-1
4
6
8
10
12
14
16
18
20
Time (hours)

(d)

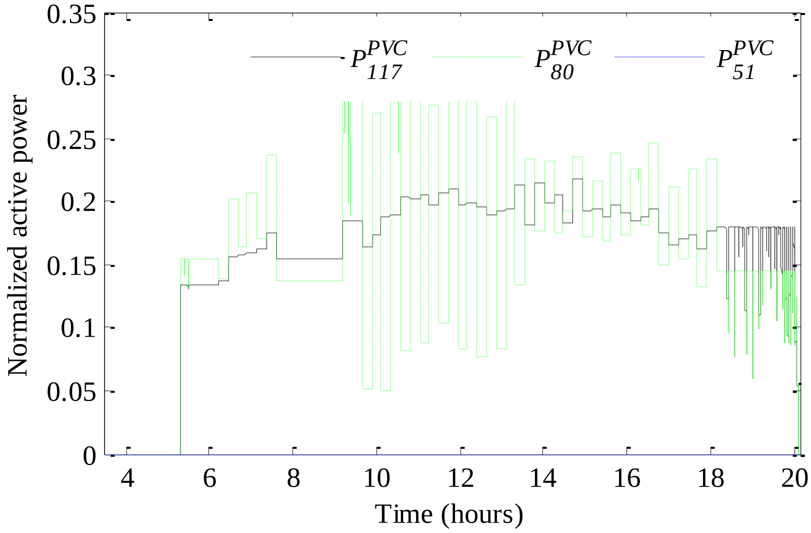
P_{117}^{PVC}
P_{80}^{PVC}
P_{51}^{PVC}
Normalized active power
0.35
0.3
0.25
0.2
0.15
0.1
0.05
0
4
6
8
10
12
14
16
18
20
Time (hours)

(e)

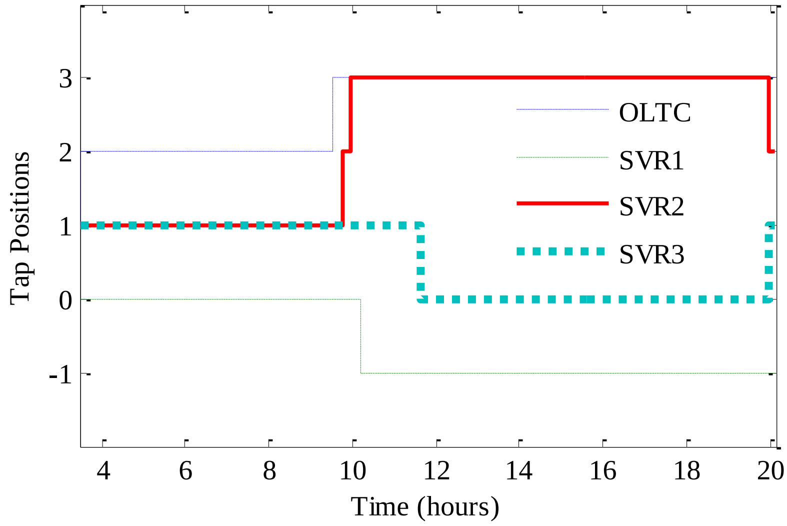

(f)

Fig. 9. Results of the proposed control strategy. (a) Voltage profiles of Area 1, (b) Voltage profiles of Area 2, (c) Voltage profiles of Area 3, (d) active PV power curtailment, (e) PV reactive power, (f) transformer taps. Bold lines in (a,b,c) are PCC voltages.

5.5 Comparison with Other Control Strategies

Table 1 compares the results of the proposed strategy, the base case, the R/X control strategy, and two other existing strategies (strategies 1 and 2). Strategies 1 and 2 utilize a centralized control scheme, but they are not enabled with the LVF mitigation capability. Another difference is that Strategy 1 optimizes the reactive power of PV inverters while Strategy 2 supplies full reactive power according to the spare capacity of the interfacing inverter.

To quantize the improvement in LVF, we calculate a voltage flicker index (VFI) of the three conditions, which is calculated by the average of voltage variations for all time durations during the studied period. Also, the maximum voltage flicker index (MVFI) is computed during the studied period. VFI and MVFI formulae at bus r can be expressed as follows:

$$VFI_r = \frac{1}{N}\sum_{t_m \in T}\left|V_r^{Abs}(t_m) - V_r^{Abs}(t_{m-1})\right| \qquad (35)$$

$$MVFI_r = \max_{t_m}\left|V_r^{Abs}(t_m) - V_r^{Abs}(t_{m-1})\right| \qquad (36)$$

The maximum values of VFI and MVFI at all buses are 5.1e^{-3} and 0.050% for the base case while they are reduced to 1.9 e^{-3} and 0.020% by the R/X control. In turn, these figures are significantly reduced to be only 0.3e^{-3} and 0.003% by the proposed strategy. Strategies 1 and 2 have the highest VFI and MVFI values as they do not have the LVF mitigation capability. Regarding VV, a VV index (VVI) is equal to zero for all strategies (except the base case), implying the voltages are kept within limits. Furthermore, the proposed strategy has low TMRs compared with other strategies.

Table 1

Results of the control strategies

Strategy	VFI	MVFI (%)	VVI	TMR
Base	5.1e^{-3}	0.050	1	-
R/X Strategy	1.9e^{-3}	0.019	0	12
Strategy 1	5.7e^{-3}	0.110	0	13
Strategy 2	5.5e^{-3}	0.089	0	37
Proposed strategy	0.3e^{-3}	0.003	0	11

5.6 Assessing the proposed voltage control strategy with High number of PV units

Here, the proposed control strategy is tested with 15 PV units in the 119-bus test system where five PV units are assumed to be connected at each area. Specifically, the buses interconnected with PV are 50, 51, 52, 53, 54, 74, 76, 78, 79, 80, 111, 114, 115, 117, and 118. Fig. 10 shows the results of the proposed control strategy in terms of voltage profiles in areas 1-3 during the day. It is clear that the proposed control strategy can solve both VD and VF problems for all buses in the three areas as the voltages are kept within the lower/upper limits, and the voltages are greatly smoothed compared with the base case. Table 2 compares the results of the proposed strategy with 3 PV units and 15 PV units. The proposed control strategy can solve the VD problem even with the higher number of PV units where VVI is zero. However, higher VFI and MVFI values are noticed in the case of accommodating 15 PV units compared with the lower PV number case. Further, the TMR value with 15 PV units is higher than that with 3 PV units. This analysis implies that increasing the PV units in distribution systems have great impacts on the voltage profile condition and the operation of voltage control devices.

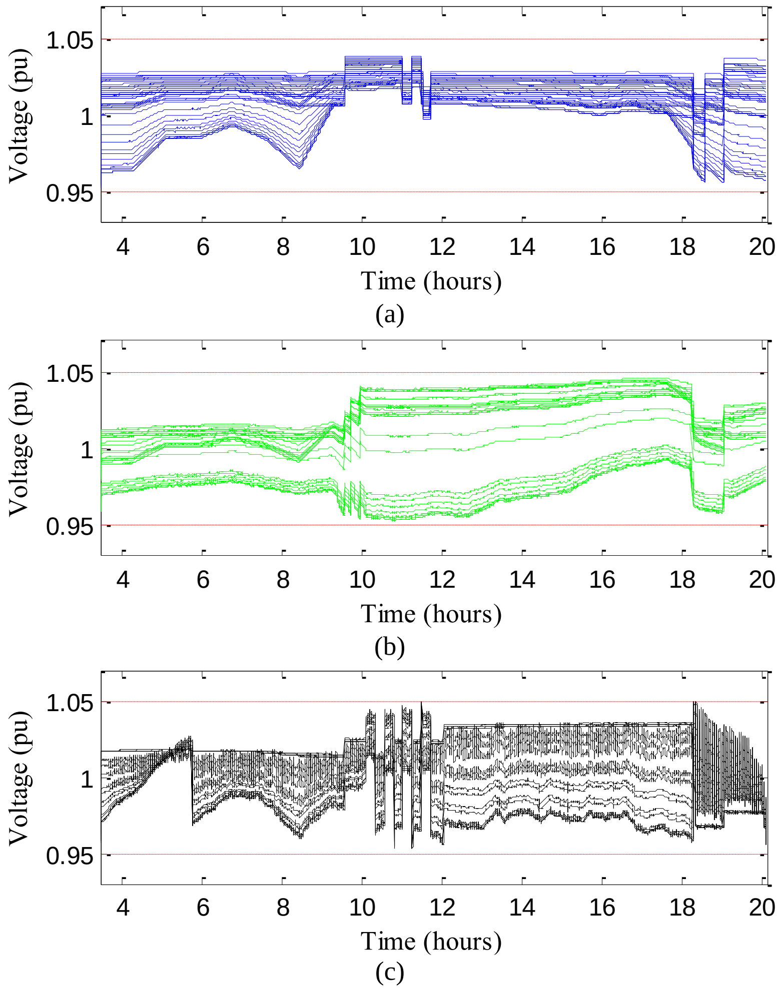

Fig. 10. Voltage profiles of the three areas with 15 PV units by the proposed control strategy. (a) Voltage profiles of Area 1, (b) Voltage profiles of Area 2, (c) Voltage profiles of Area 3.

Table 2

Results of the proposed control strategy with 3 and 15 PV units

Number of PV	VFI	MVFI (%)	VVI	TMR
3 PVs	$0.3e^{-3}$	0.003	0	11
15 PVs	$8.2e^{-3}$	0.083	0	44

6. Conclusions

Various operational problems are common in PV-rich distribution systems, such as VD, VF, high PV active power curtailment, and excessive tap operations of OLTC and SVRs. In this work, an optimal control strategy has been proposed to solve these problems. Intensive simulations with fine resolutions of the dataset have been carried out to validate and demonstrate the effectiveness of the proposed strategy. The features of the proposed method are summarized here.

- The proposed analytical expressions employed in the LC units for VF minimization can accurately optimize the smart functions of the PV inverter to significantly solve the VF problem compared with existing formulations.
- The proposed analytical expressions employed in LC and AC units for minimizing VD is accurate compared to exact solutions computed by search-based methods.
- The proposed control strategy can minimize VD and VF while optimizing the total active curtailed power of multiple PV units and tap operations of transformers by the CC unit.

The proposed strategy with the unified treatment of VD and VF and coordinated control actions can greatly facilitate the integration of high PV penetrations in distribution systems. The future study will be focused on considering various types of renewable DERs, e.g., wind power generation systems and energy storage.

References

[1] Mohandes B, Moursi MS El, Hatziargyriou N, Khatib S El. A Review of Power System Flexibility With High Penetration of Renewables. IEEE Trans Power Syst 2019;34:3140–55. https://doi.org/10.1109/TPWRS.2019.2897727.

[2] Haghdadi N, Bruce A, MacGill I, Passey R. Impact of Distributed Photovoltaic Systems on Zone Substation Peak Demand. IEEE Trans Sustain Energy 2018;9:621–9. https://doi.org/10.1109/TSTE.2017.2751647.

[3] Liang X. Emerging Power Quality Challenges Due to Integration of Renewable Energy Sources. IEEE Trans Ind Appl 2017;53:855–66. https://doi.org/10.1109/TIA.2016.2626253.

[4] Moosavian SM, Rahim NA, Selvaraj J, Solangi KH. Energy policy to promote photovoltaic generation. Renew Sustain Energy Rev 2013;25:44–58. https://doi.org/10.1016/J.RSER.2013.03.030.

[5] Ahn H, Rim D, Pavlak GS, Freihaut JD. Uncertainty analysis of energy and economic performances of hybrid solar photovoltaic and combined cooling, heating, and power (CCHP + PV) systems using a Monte-Carlo method. Appl Energy 2019;255:113753. https://doi.org/10.1016/J.APENERGY.2019.113753.

[6] Mahmoud K, Abdel-Nasser M. Fast-yet-Accurate Energy Loss Assessment Approach for Analyzing/Sizing PV in Distribution Systems using Machine Learning. IEEE Trans Sustain Energy 2018:1–1. https://doi.org/10.1109/TSTE.2018.2859036.

[7] Wang S, Chen S, Ge L, Wu L. Distributed Generation Hosting Capacity Evaluation for

Distribution Systems Considering the Robust Optimal Operation of OLTC and SVC. IEEE Trans Sustain Energy 2016;7:1111–23. https://doi.org/10.1109/TSTE.2016.2529627.

[8] Mahmoud K, Hussein MM, Abdel-Nasser M, Lehtonen M. Optimal Voltage Control in Distribution Systems With Intermittent PV Using Multiobjective Grey-Wolf-Lévy Optimizer. IEEE Syst J 2019:1–11. https://doi.org/10.1109/JSYST.2019.2931829.

[9] Elvira-Ortiz DA, Morinigo-Sotelo D, Duque-Perez O, Jaen-Cuellar AY, Osornio-Rios RA, Romero-Troncoso R de J. Methodology for Flicker Estimation and Its Correlation to Environmental Factors in Photovoltaic Generation. IEEE Access 2018;6:24035–47. https://doi.org/10.1109/ACCESS.2018.2829148.

[10] Mahmoud K, Lehtonen M. Simultaneous Allocation of Multi-Type Distributed Generations and Capacitors Using Generic Analytical Expressions. IEEE Access 2019;7:182701–10. https://doi.org/10.1109/access.2019.2960152.

[11] Roy Ghatak S, Sannigrahi S, Acharjee P. Multi-Objective Approach for Strategic Incorporation of Solar Energy Source, Battery Storage System, and DSTATCOM in a Smart Grid Environment. IEEE Syst J 2018;2:1–12. https://doi.org/10.1109/JSYST.2018.2875177.

[12] Ma C, Menke J-H, Dasenbrock J, Braun M, Haslbeck M, Schmid K-H. Evaluation of energy losses in low voltage distribution grids with high penetration of distributed generation. Appl Energy 2019;256:113907. https://doi.org/10.1016/J.APENERGY.2019.113907.

[13] Adewuyi OB, Lotfy ME, Akinloye BO, Rashid Howlader HO, Senjyu T, Narayanan K. Security-constrained optimal utility-scale solar PV investment planning for weak

grids: Short reviews and techno-economic analysis. Appl Energy 2019;245:16–30. https://doi.org/10.1016/J.APENERGY.2019.04.008.

[14] Wang L, Yan R, Saha TK. Voltage regulation challenges with unbalanced PV integration in low voltage distribution systems and the corresponding solution. Appl Energy 2019;256:113927. https://doi.org/10.1016/J.APENERGY.2019.113927.

[15] Yan R, Marais B, Saha TK. Impacts of residential photovoltaic power fluctuation on on-load tap changer operation and a solution using DSTATCOM. Electr Power Syst Res 2014;111:185–93. https://doi.org/10.1016/J.EPSR.2014.02.020.

[16] Nousdilis AI, Christoforidis GC, Papagiannis GK. Active power management in low voltage networks with high photovoltaics penetration based on prosumers' self-consumption. Appl Energy 2018;229:614–24. https://doi.org/10.1016/j.apenergy.2018.08.032.

[17] Jannesar MR, Sedighi A, Savaghebi M, Guerrero JM. Optimal placement, sizing, and daily charge/discharge of battery energy storage in low voltage distribution network with high photovoltaic penetration. Appl Energy 2018;226:957–66. https://doi.org/10.1016/j.apenergy.2018.06.036.

[18] Wang X, Wang C, Xu T, Guo L, Li P, Yu L, et al. Optimal voltage regulation for distribution networks with multi-microgrids. Appl Energy 2018;210:1027–36. https://doi.org/10.1016/j.apenergy.2017.08.113.

[19] Li P, Ji H, Yu H, Zhao J, Wang C, Song G, et al. Combined decentralized and local voltage control strategy of soft open points in active distribution networks. Appl Energy 2019;241:613–24. https://doi.org/10.1016/j.apenergy.2019.03.031.

[20] Bai L, Jiang T, Li F, Chen H, Li X. Distributed energy storage planning in soft open point based active distribution networks incorporating network reconfiguration and DG reactive power capability. Appl Energy 2018;210:1082–91. https://doi.org/10.1016/j.apenergy.2017.07.004.

[21] Almasalma H, Claeys S, Deconinck G. Peer-to-peer-based integrated grid voltage support function for smart photovoltaic inverters. Appl Energy 2019;239:1037–48. https://doi.org/10.1016/j.apenergy.2019.01.249.

[22] Susanto J, Shahnia F, Ludwig D. A framework to technically evaluate integration of utility-scale photovoltaic plants to weak power distribution systems. Appl Energy 2018;231:207–21. https://doi.org/10.1016/j.apenergy.2018.09.130.

[23] Gandhi O, Rodríguez-Gallegos CD, Zhang W, Srinivasan D, Reindl T. Economic and technical analysis of reactive power provision from distributed energy resources in microgrids. Appl Energy 2018;210:827–41. https://doi.org/10.1016/j.apenergy.2017.08.154.

[24] IEEE Standard for Interconnecting Distributed Resources with Electric Power Systems - Amendment 1. IEEE Std 1547a-2014 (Amendment to IEEE Std 1547-2003) 2014:1–16. https://doi.org/10.1109/IEEESTD.2014.6818982.

[25] Reza Malekpour A, Pahwa A. A Dynamic Operational Scheme for Residential PV Smart Inverters. IEEE Trans Smart Grid 2017;8:2258–67. https://doi.org/10.1109/TSG.2016.2521367.

[26] Sangwongwanich A, Yang Y, Sera D, Blaabjerg F, Zhou D. On the Impacts of PV Array Sizing on the Inverter Reliability and Lifetime. IEEE Trans Ind Appl 2018;54:3656–67. https://doi.org/10.1109/TIA.2018.2825955.

[27] Ali A, Raisz D, Mahmoud K. Optimal oversizing of utility-owned renewable DG inverter for voltage rise prevention in MV distribution systems. Int J Electr Power Energy Syst 2019;105:500–13. https://doi.org/10.1016/J.IJEPES.2018.08.040.

[28] Vahan G, Booth S. Review of PREPA technical requirements for interconnecting wind and solar generation. Natl Renew Energy Lab (NREL), Tech Rep NREL/TP-5D00-57089 2013:72. https://www.osti.gov/biblio/1260328 (accessed July 8, 2019).

[29] Weckx S, Driesen J. Optimal Local Reactive Power Control by PV Inverters. IEEE Trans Sustain Energy 2016;7:1624–33. https://doi.org/10.1109/TSTE.2016.2572162.

[30] Weckx S, Gonzalez C, Driesen J. Combined Central and Local Active and Reactive Power Control of PV Inverters. IEEE Trans Sustain Energy 2014;5:776–84. https://doi.org/10.1109/TSTE.2014.2300934.

[31] Su X, Masoum MAS, Wolfs PJ. Optimal PV Inverter Reactive Power Control and Real Power Curtailment to Improve Performance of Unbalanced Four-Wire LV Distribution Networks. IEEE Trans Sustain Energy 2014;5:967–77. https://doi.org/10.1109/TSTE.2014.2313862.

[32] Zeraati M, Golshan MEH, Guerrero JM. A Consensus-Based Cooperative Control of PEV Battery and PV Active Power Curtailment for Voltage Regulation in Distribution Networks. IEEE Trans Smart Grid 2017;3053:1–1. https://doi.org/10.1109/TSG.2017.2749623.

[33] Tonkoski R, Lopes LAC, El-Fouly THM. Coordinated active power curtailment of grid connected PV inverters for overvoltage prevention. IEEE Trans Sustain Energy 2011;2:139–47. https://doi.org/10.1109/TSTE.2010.2098483.

[34] Zhao B, Xu Z, Xu C, Wang C, Lin F. Network Partition Based Zonal Voltage Control for Distribution Networks with Distributed PV Systems. IEEE Trans Smart Grid 2017;PP:1–1. https://doi.org/10.1109/TSG.2017.2648779.

[35] Rahimi K, Omran S, Dilek M, Broadwater R. Computation of Voltage Flicker With Cloud Motion Simulator. IEEE Trans Ind Appl 2018;54:2628–36. https://doi.org/10.1109/TIA.2017.2787621.

[36] Omran WA, Kazerani M, Salama MMA. Investigation of methods for reduction of power fluctuations generated from large grid-connected photovoltaic systems. IEEE Trans Energy Convers 2011;26:318–27. https://doi.org/10.1109/TEC.2010.2062515.

[37] Trindade FCL, Ferreira TSD, Lopes MG, Freitas W. Mitigation of Fast Voltage Variations During Cloud Transients in Distribution Systems With PV Solar Farms. IEEE Trans Power Deliv 2017;32:921–32. https://doi.org/10.1109/TPWRD.2016.2562922.

[38] Alam, M. J. E., K. M. Muttaqi DS. A Novel Approach for Ramp-Rate Control of Solar PV Using Energy Storage to Mitigate Output Fluctuations Caused by Cloud Passing. IEEE Trans Energy Convers 2014;29:507–18. https://doi.org/10.1109/TEC.2014.2304951.

[39] Yuan Y, Sun C, Li M, Choi SS, Li Q. Determination of optimal supercapacitor-lead-acid battery energy storage capacity for smoothing wind power using empirical mode decomposition and neural network. Electr Power Syst Res 2015;127:323–31. https://doi.org/10.1016/J.EPSR.2015.06.015.

[40] Datta M, Senjyu T, Yona A, Funabashi T, Chul-Hwan Kim. A Frequency-Control Approach by Photovoltaic Generator in a PV–Diesel Hybrid Power System. IEEE

Trans Energy Convers 2011;26:559–71. https://doi.org/10.1109/TEC.2010.2089688.

[41] Ali A, Raisz D, Mahmoud K. Sensitivity-based and optimization-based methods for mitigating voltage fluctuation and rise in the presence of PV and PHEVs. Int Trans Electr Energy Syst 2017;27:e2456. https://doi.org/10.1002/etep.2456.

[42] Ali A, Raisz D, Mahmoud K. Voltage fluctuation smoothing in distribution systems with RES considering degradation and charging plan of EV batteries. Electr Power Syst Res 2019;176:105933. https://doi.org/10.1016/j.epsr.2019.105933.

[43] Bedawy A, Yorino N, Mahmoud K, Zoka Y, Sasaki Y. Optimal Voltage Control Strategy for Voltage Regulators in Active Unbalanced Distribution Systems Using Multi-Agents. IEEE Trans Power Syst 2019:1–1. https://doi.org/10.1109/TPWRS.2019.2942583.

[44] Omran WA, Kazerani M, Salama MMA. Investigation of Methods for Reduction of Power Fluctuations Generated From Large Grid-Connected Photovoltaic Systems. IEEE Trans Energy Convers 2011;26:318–27. https://doi.org/10.1109/TEC.2010.2062515.

[45] Zhou S, Brown MA. Smart meter deployment in Europe: A comparative case study on the impacts of national policy schemes. J Clean Prod 2017;144:22–32. https://doi.org/10.1016/J.JCLEPRO.2016.12.031.

[46] Yorino N, Mahmoud K. Robust quadratic-based BFS power flow method for multi-phase distribution systems. IET Gener Transm Distrib 2016;10:2240–50. https://doi.org/10.1049/iet-gtd.2015.1518.

[47] Turitsyn K, Sulc P, Backhaus S, Chertkov M. Options for Control of Reactive Power

by Distributed Photovoltaic Generators. Proc IEEE 2011;99:1063–73. https://doi.org/10.1109/JPROC.2011.2116750.

[48] Jafary P, Raipala O, Repo S, Salmenpera M, Seppala J, Koivisto H, et al. Secure layer 2 tunneling over IP for GOOSE-based logic selectivity. Proc. IEEE Int. Conf. Ind. Technol., Toronto, ON: 2017, p. 609–14. https://doi.org/10.1109/ICIT.2017.7915428.

[49] Arshad A, Lehtonen M. A comprehensive voltage control strategy with voltage flicker compensation for highly PV penetrated distribution networks. Electr Power Syst Res 2019;172:105–13. https://doi.org/10.1016/j.epsr.2019.02.019.

[50] Zhang D, Fu Z, Zhang L. An improved TS algorithm for loss-minimum reconfiguration in large-scale distribution systems. Electr Power Syst Res 2007;77:685–94. https://doi.org/10.1016/j.epsr.2006.06.005.

[51] High-Resolution Solar Radiation Datasets. Natural Resources Canada. https://www.nrcan.gc.ca/energy/renewable-electricity/solar-photovoltaic/18409 (accessed August 5, 2019).